MAVEN observations of a giant ionospheric flux rope near Mars resulting from interaction between the crustal and interplanetary draped magnetic fields

Takuya Hara, David A. Brain, David L. Mitchell, Janet G. Luhmann, Kanako Seki, Hiroshi Hasegawa, James P. Mcfadden, Jasper S. Halekas, Jared R. Espley, Yuki Harada, et al.

AGU PUBLICATIONS

JGR

Journal of Geophysical Research: Space Physics

RESEARCH ARTICLE
10.1002/2016JA023347

Special Section:
Major Results From the MAVEN Mission to Mars

MAVEN observations of a giant ionospheric flux rope near Mars resulting from interaction between the crustal and interplanetary draped magnetic fields

Takuya Hara[1], David A. Brain[2], David L. Mitchell[1], Janet G. Luhmann[1], Kanako Seki[3], Hiroshi Hasegawa[4], James P. Mcfadden[1], Jasper S. Halekas[5], Jared R. Espley[6], Yuki Harada[1], Roberto Livi[1], Gina A. DiBraccio[6], John E. P. Connerney[6], Christian Mazelle[7,8], Laila Andersson[2], and Bruce M. Jakosky[2]

[1]Space Sciences Laboratory, University of California, Berkeley, California, USA, [2]Laboratory for Atmospheric and Space Physics, University of Colorado Boulder, Boulder, Colorado, USA, [3]Department of Earth and Planetary Science, Graduate School of Science, University of Tokyo, Tokyo, Japan, [4]Institute of Space and Astronautical Science, Japan Aerospace Exploration Agency, Sagamihara, Japan, [5]Department of Physics and Astronomy, University of Iowa, Iowa City, Iowa, USA, [6]NASA Goddard Space Flight Center, Greenbelt, Maryland, USA, [7]CNRS, Institut de Recherche en Astrophysique et Planétologie, Toulouse, France, [8]Université Paul Sabatier, Toulouse, France

Key Points:
- MAVEN observed a giant flux rope near the subsolar point of the Martian ionosphere, downstream from the strong crustal fields
- The observed giant ionospheric flux rope was formed via interactions between the local crustal and overlaid draped magnetic fields
- The event was observed during the ICME passage by Mars, indicating that the ICME played a role in forming the observed giant flux rope

Correspondence to:
T. Hara,
hara@ssl.berkeley.edu

Citation:
Hara, T., et al. (2017), MAVEN observations of a giant ionospheric flux rope near Mars resulting from interaction between the crustal and interplanetary draped magnetic fields, *J. Geophys. Res. Space Physics*, *122*, 828–842, doi:10.1002/2016JA023347.

Received 24 AUG 2016
Accepted 7 DEC 2016
Accepted article online 13 DEC 2016
Published online 3 JAN 2017

Abstract We present Mars Atmosphere and Volatile EvolutioN (MAVEN) observations of a giant magnetic flux rope in the Martian dayside ionosphere. The flux rope was observed at an altitude of <300 km, downstream from strong subsolar crustal magnetic fields. The peak field amplitude was ~200 nT, resulting in the largest difference between the observed magnetic field strength and a model for crustal magnetic fields of the entire MAVEN primary science phase. MAVEN detected planetary ions, including H^+, O^+, and O_2^+, across the structure. The axial orientation estimated for the flux rope indicates that it likely formed as a result of interactions between the local crustal and overlaid draped interplanetary magnetic fields. Pitch angle distributions of ionospheric photoelectrons imply that this structure is connected to the Martian upper atmosphere. However, the flux rope is not present in observations at the next commensurable orbit crossing (approximately two Martian days later), implying that it eventually detaches from the atmosphere and is carried downstream. The flux rope observations occurred during an interplanetary coronal mass ejection event at Mars, suggesting that the disturbed upstream state played a role in allowing the interplanetary magnetic field to penetrate deeper into the Martian ionosphere than is typical, allowing the formation of the flux rope.

1. Introduction

Flux ropes are fundamental twisted helical magnetic field structures [e.g., *Russell and Elphic*, 1979a]. They have been detected throughout the solar system, including Earth [e.g., *Russell and Elphic*, 1979b; *Hasegawa et al.*, 2010], Mercury [e.g., *Slavin et al.*, 2009; *Imber et al.*, 2014], and the Jovian planets [e.g., *Walker and Russell*, 1985; *Jasinski et al.*, 2016], which possess a global intrinsic dipole magnetic field. One key issue associated with the flux rope studies is to understand how flux ropes are formed in the solar system. Flux ropes have been currently postulated to form as a result of magnetic reconnection between interplanetary magnetic field (IMF) and intrinsic magnetic field.

On the other hand, they have been also measured around the Martian plasma environment, even though Mars does not possess a global intrinsic magnetic field [e.g., *Cloutier et al.*, 1999; *Vignes et al.*, 2004]. The candidate sources of the Martian flux ropes are due to not only the IMF draped around Mars but also the highly asymmetric localized crustal magnetic fields [e.g., *Acuña et al.*, 1998, 1999]. A large number of flux ropes had been detected by Mars Global Surveyor (MGS) in the Martian ionosphere [e.g., *Cloutier et al.*, 1999; *Vignes et al.*, 2004; *Briggs et al.*, 2011]. Indeed, Mars Atmosphere and Volatile EvolutioN (MAVEN) also successfully measures several flux ropes around Mars even at altitudes higher than 1000 km [*Hara et al.*, 2015; *DiBraccio et al.*, 2015]. Their peak field amplitudes are mostly weaker than ~30 nT [e.g., *Vignes et al.*, 2004]. Meanwhile, strong axial field flux ropes (~80 nT) have recently been discovered in the magnetosheath, in particular, during the passage of the interplanetary coronal mass ejection (ICME) [*Hara et al.*, 2016].

Furthermore, large-scale ionospheric flux ropes with a peak field stronger than 100 nT were measured by MGS downstream from the strong crustal fields [e.g., *Brain et al.*, 2010; *Morgan et al.*, 2011; *Hara et al.*, 2014a]. *Brain et al.* [2010] proposed that the dayside crustal field lines are stretched tailward because of the solar wind flow and may detach via magnetic reconnection. *Beharrell and Wild* [2012], who found magnetic field enhancements mostly due to flux ropes, were repeatedly detected by MGS around the terminator region in the southern hemisphere. They were also downstream from the strong crustal fields. Based on candidate lists done by *Beharrell and Wild* [2012], *Soobiah et al.* [2014] further investigated one large-scale flux rope in conjunction with the Mars Express (MEX) measurements, because MEX was occasionally close to MGS within 500 km and 40 min. *Beharrell and Wild* [2012] noticed they can be created through internal reconnections between neighboring crustal fields, whereby field lines are stretched and overlay neighboring crustal fields. *Hara et al.* [2014b] statistically investigated possible formation processes of ionospheric flux ropes observed by MGS around the southern polar region downstream from the strong crustal fields, based on their spatial properties inferred from the Grad-Shafranov reconstruction (GSR) technique. This technique is capable of recovering the two-dimensional axial field structures and axial orientations of flux ropes based on single spacecraft measurements [e.g., *Hau and Sonnerup*, 1999; *Hu and Sonnerup*, 2002]. *Hara et al.* [2014b] suggested that IMF draped around Mars can play a significant role, because they can be created in consequence of interactions between the local crustal and overlaid draped magnetic fields.

However, MGS had some limitations to further understand possible formation processes of the Martian flux ropes. For example, since the MGS was usually well below the Martian bow shock during its mapping phase [*Albee et al.*, 2001], it is not straightforward to deduce the IMF orientations draped around Mars from MGS [*Brain et al.*, 2006]. Therefore, possible scenarios on how flux ropes are created in the Martian plasma environment are still under debate. On the other hand, MAVEN enables the measurements in various plasma regimes including the upstream solar wind, magnetosheath, induced magnetosphere, and down to the Martian ionosphere [*Jakosky et al.*, 2015]. The MAVEN comprehensive particle and field instruments allow us to reveal unprecedented behaviors of the Martian flux ropes [*Hara et al.*, 2015].

In this paper, we first present clear MAVEN observations of a giant ionospheric flux rope in the vicinity of the subsolar crustal magnetic fields. MAVEN observations together with the spatial structure inferred from the GSR technique show the more convincing evidence than ever that a giant ionospheric flux rope can be formed via multiple *X* line reconnection between the local crustal magnetic fields and overlaid interplanetary magnetic fields draped around Mars.

2. Identification of Martian Ionospheric Flux Ropes

In order to surely identify the Martian ionospheric flux ropes from the spacecraft measurements, it is essential to distinguish between ionospheric flux ropes and the local crustal fields themselves. In previous studies based on the MGS observations, they compared the spacecraft magnetic field observations with the modeled crustal field predictions [e.g., *Brain et al.*, 2010; *Beharrell and Wild*, 2012; *Hara et al.*, 2014b]. MGS fixed its local time of 2 A.M./2 P.M. at an altitude of ~400 km during its mapping phase [*Albee et al.*, 2001]. On the other hand, MAVEN has an elliptical orbit, designed to precess rapidly around Mars with a periapsis (apoapsis) altitude of ~150 (~6200) km [*Jakosky et al.*, 2015]. In addition, present crustal field models are totally based on the MGS measurements at an altitude of ~400 km [e.g., *Cain et al.*, 2003; *Morschhauser et al.*, 2014]; therefore, there might be some ambiguity in the reliability of these models at altitudes lower than 400 km.

Taking into account the differences of the orbital configuration between MGS and MAVEN, here we propose the methodology to surely identify the ionospheric flux ropes from the MAVEN magnetic field data. Comparing the durations between the MAVEN orbital period (~4.5 h) and the Martian rotation period (~24.66 h), it just takes approximately two Martian days for MAVEN to orbit Mars 11 times. It means that quite a similar orbital configurations relative to the local crustal fields are available every 11 MAVEN orbits (approximately two Martian days). In this paper, here we call this orbital feature "11:2 commensurability."

For example, if we find a candidate ionospheric flux rope event from the MAVEN data, we compare the MAVEN magnetic field data obtained in adjacent "commensurable" orbits, which are 11 MAVEN orbits before and after the event. Given that similar magnetic field signatures are seen in these adjacent commensurable orbits, we can regard this event as a stable structure like a crustal magnetic field. In contrast, in case we cannot find any similar magnetic field signatures in the adjacent commensurable orbits, we can conclude that this event is a transient structure like a magnetic flux rope. The actual spatial difference between these commensurable

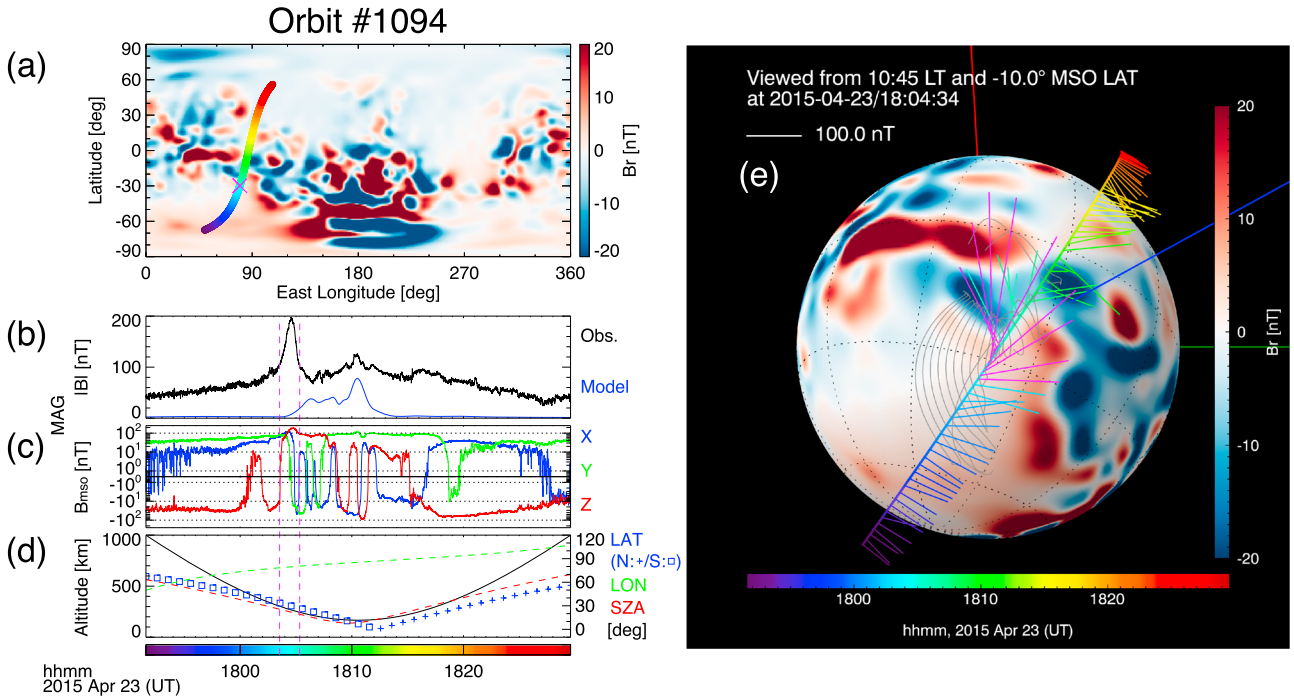

Figure 1. An overview of magnetic field measurements where MAVEN traversed at an altitude lower than 1000 km for orbit #1094: (a) The spacecraft trajectory (rainbow line) projected onto the modeled crustal field map at 400 km [*Morschhauser et al.*, 2014] during the time interval shown as a color bar at the bottom of Figure 1d. The time profiles of (b) the observed magnetic field strength (|***B***|: black) together with the crustal field model (blue) [*Morschhauser et al.*, 2014], (c) the observed magnetic field components in the MSO coordinates, and (d) the spacecraft altitude (organized in the left *y* axis: black) and foot points (organized in the right *y* axis), including the geographic latitude (LAT: blue), longitude (LON: green), and solar zenith angle (SZA: red). (e) The three-dimensional whisker plots of the observed magnetic fields along the spacecraft trajectory (rainbow), viewed from the local time of 10:45 and the MSO latitude of −10°. Blue, green, and red solid lines are the projected X_{mso}, Y_{mso}, and Z_{mso} axes, respectively. The correspondent times at the rainbow trajectory are identical to Figures 1a. The blue-red background is also the same as in Figure 1a; however, it is projected on the globe surface at the time as noted on Figure 1e. The whisker length is proportional to the field strength. A giant ionospheric flux rope was observed between two magenta dashed vertical lines between Figures 1b and 1d.

orbits is smaller than ~300 km. Analogous investigations were performed solely for the MGS measurements by *Soobiah et al.* [2014].

Figure 1 shows an overview of the MAVEN magnetic field measurements when the spacecraft is at altitudes lower than 1000 km on orbit #1094. During this time interval, MAVEN was mainly traveling in the Martian dayside induced magnetosphere and ionosphere from the southern hemisphere (blue squares in Figure 1d) to the northern hemisphere (blue pluses in Figure 1d). The MAVEN orbital foot points and three-dimensional trajectory, projected onto the blue-red modeled crustal field map at 400 km [*Morschhauser et al.*, 2014], are displayed as the rainbow curve in Figures 1a and 1e. The MAVEN periapsis was closed to the subsolar point. Figures 1a and 1e indicate that MAVEN flew over the equator moderate crustal field region around the periapsis. However, MAVEN abruptly observed the sharp magnetic field enhancement with a peak field of ~200 nT, even though the modeled crustal field is predicted rather weak between two magenta dashed vertical lines in Figures 1b–1d. The event location is also marked as the magenta cross (whiskers) in Figure 1a (1e). The event geometry relative to the neighboring crustal fields is similar to the previous MGS measurements [e.g., *Brain et al.*, 2010; *Hara et al.*, 2014a]. However, this event was detected around the subsolar point at an altitude lower than 300 km. Note that a bisymmetric logarithmic axis is adopted in Figure 1c, enabling us to display both positive and negative values on the logarithmic scale, so that it makes easier to see the dynamic variations of the magnetic field, because the observed magnetic field variations are in the range of from plus/minus a few tens of nT to plus/minus a few hundreds of nT during the time interval of Figure 1.

Figures 2 and 3 have the same format as Figure 1; however, they are adjacent commensurable orbits #1083 (Figure 2) and #1105 (Figure 3). Indeed, the spacecraft trajectories along the geographic foot point (Figures 2a and 3a) and three-dimensional globe (Figures 2e and 3e) during adjacent commensurable orbits are quite similar to Figure 1 in terms of the local crustal magnetic configurations. However, MAVEN no longer measured such a steep enhancement in the same altitude range as in Figure 1 during these adjacent commensurable

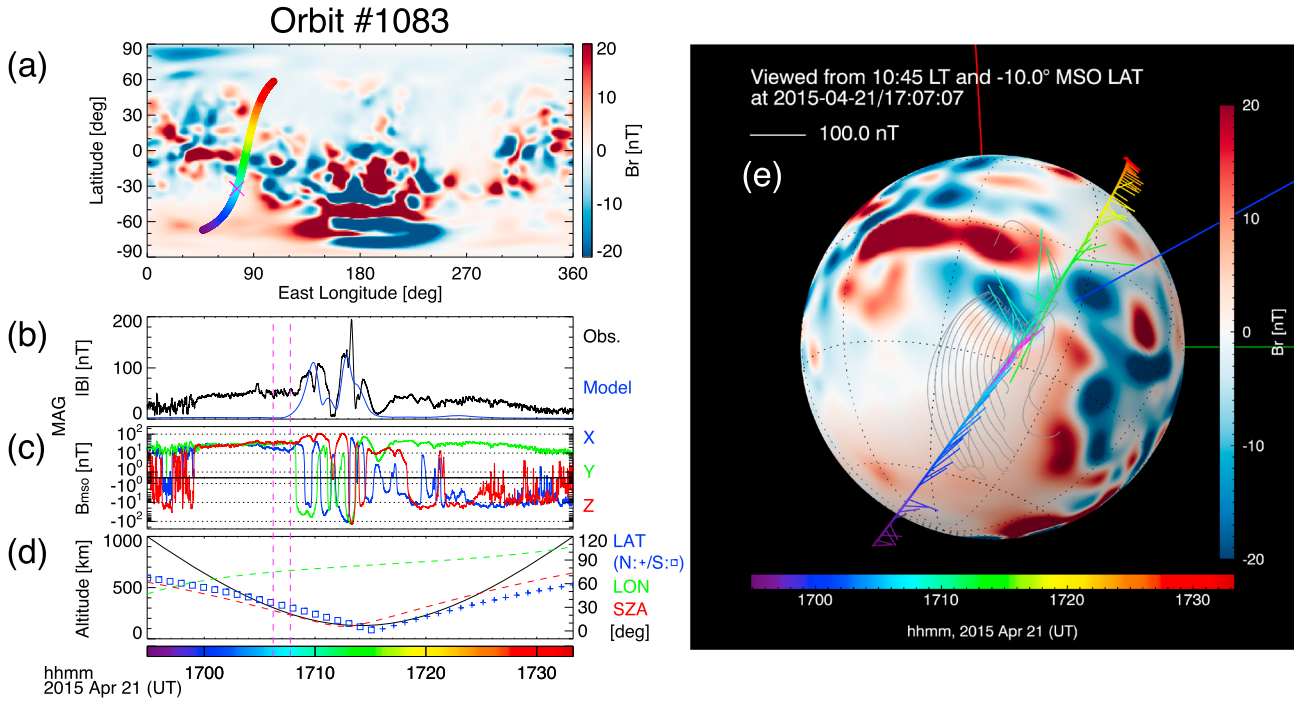

Figure 2. An overview of magnetic field measurements where MAVEN traversed at an altitude lower than 1000 km for orbit #1083: Orbit #1083 is the adjacent commensurable orbit to Figure 1 (Orbit #1094). The figure format is mostly identical to Figure 1; however, magenta cross (Figure 2a), vertical dashed lines (Figures 2b-2d), and whiskers (Figure 2e) are colored in the same altitude region, when a giant ionospheric flux rope was observed in the next commensurable orbit (see Figure 1).

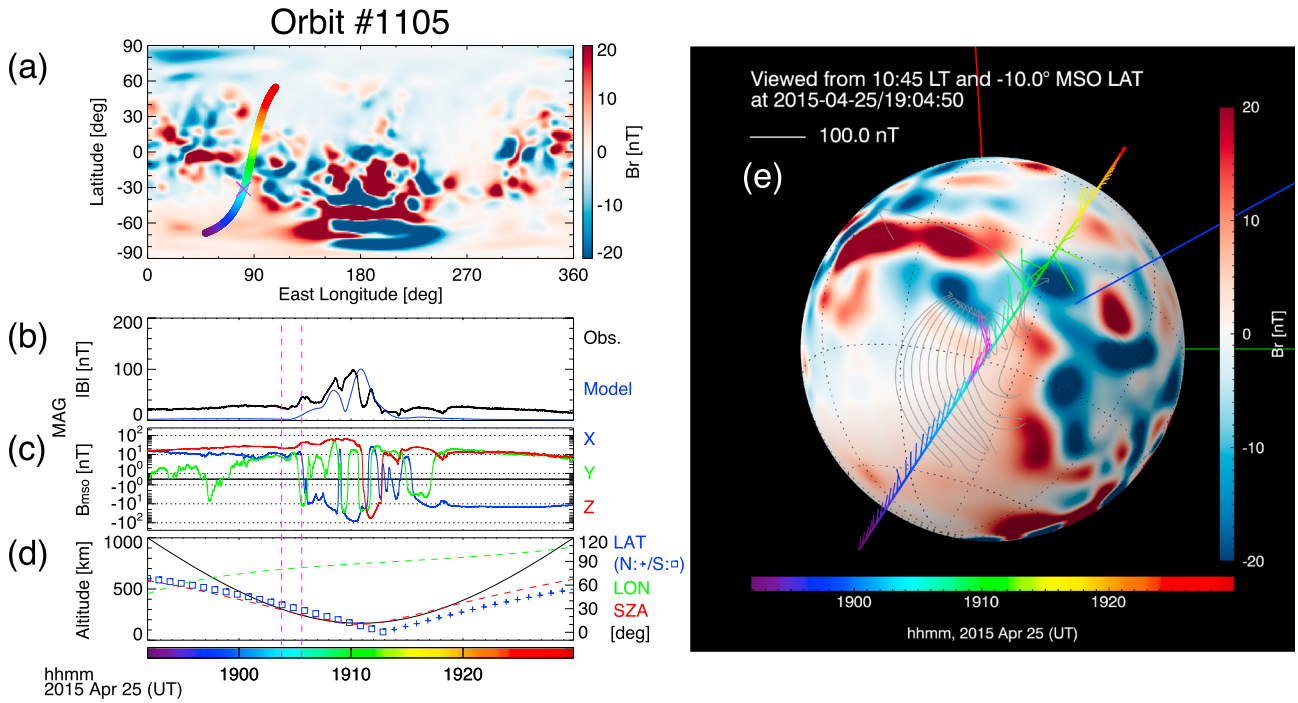

Figure 3. An overview of magnetic field measurements where MAVEN traversed at an altitude lower than 1000 km for orbit #1105: The figure format is identical to Figure 2. Orbit #1105 is the adjacent commensurable orbit to Figure 1 (Orbit #1094). A giant ionospheric flux rope was observed in the last commensurable orbit (see Figure 1).

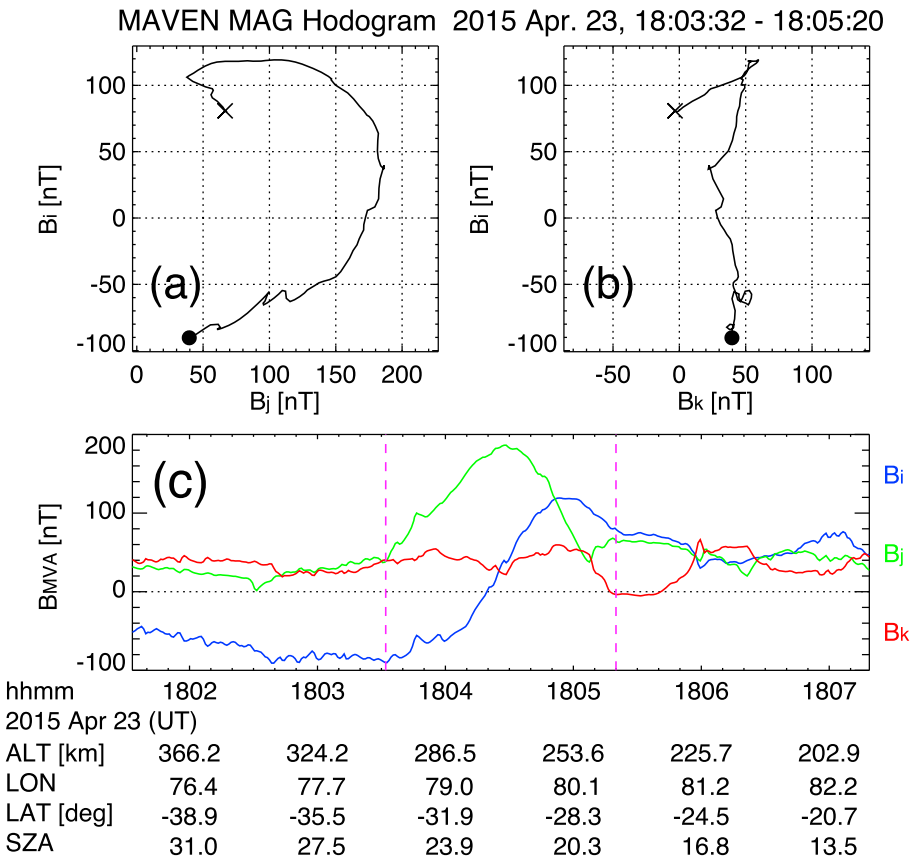

Figure 4. (a, b) The hodograms of magnetic field components in the minimum variance analysis (MVA) coordinate system, when MAVEN observed a giant ionospheric flux rope on orbit #1094. B_i, B_j, and B_k are the components along the maximum, intermediate, and minimum variance axes, respectively. Black circles (crosses) are start (end) points. (c) Time profile of the vector magnetic field transformed into the MVA coordinate system.

orbits (see Figures 2b and 3b between the two magenta dashed vertical lines). Therefore, we surely confirm that this magnetic field enhancement seen in orbit #1094 (Figure 1) is not a stable structure like a crustal flux tube but likely a transient structure like a magnetic flux rope.

We performed the minimum variance analysis (MVA) [e.g., *Sonnerup and Scheible*, 1998] by using the magnetic field measurements in the Mars-centered, Solar Orbital (MSO) coordinate system between the two magenta vertical dashed lines in Figure 1c. The MSO coordinate system is defined with the X_{mso} axis toward the Sun, the Z_{mso} axis perpendicular to the ecliptic pointing to the northern hemisphere, and the Y_{mso} axis completing the right-hand system. Figures 4a and 4b show hodograms of magnetic field components during the event in the MVA coordinate systems. Figure 4a clearly displays a smooth circular rotation in the plane perpendicular to the minimum variance direction (B_k). Figure 4c shows a time series plot of vector magnetic field during the event transformed into the MVA coordinate system. A bipolar-like magnetic field signature is well seen in the maximum variance direction (B_i). Figure 4 thus turns out to be a typical hodogram pattern of a flux rope in the MVA coordinate system [e.g., *Russell and Elphic*, 1979a; *Vignes et al.*, 2004]. The intermediate to minimum eigenvalue ratio is ~13.4, i.e., $\lambda_j/\lambda_k \simeq 13.4$, indicating that this MVA coordinate system is well determined. The MVA result thus suggests that the flux rope axis is expected to be aligned to the intermediate variance direction; $B_j = [0.749, 0.020, 0.662]$, assuming that the observed flux rope is approximately under the force-free state [e.g., *Xiao et al.*, 2004; *Rong et al.*, 2013].

3. MAVEN Observations of A Giant Ionospheric Flux Rope

Figure 5 represents time series plots of the MAVEN plasma and magnetic field measurements from the Suprathermal and Thermal Ion Composition (STATIC) analyzer [*McFadden et al.*, 2015], the Solar Wind Electron Analyzer (SWEA) [*Mitchell et al.*, 2016], and the Magnetometer (MAG) [*Connerney et al.*, 2015] across the

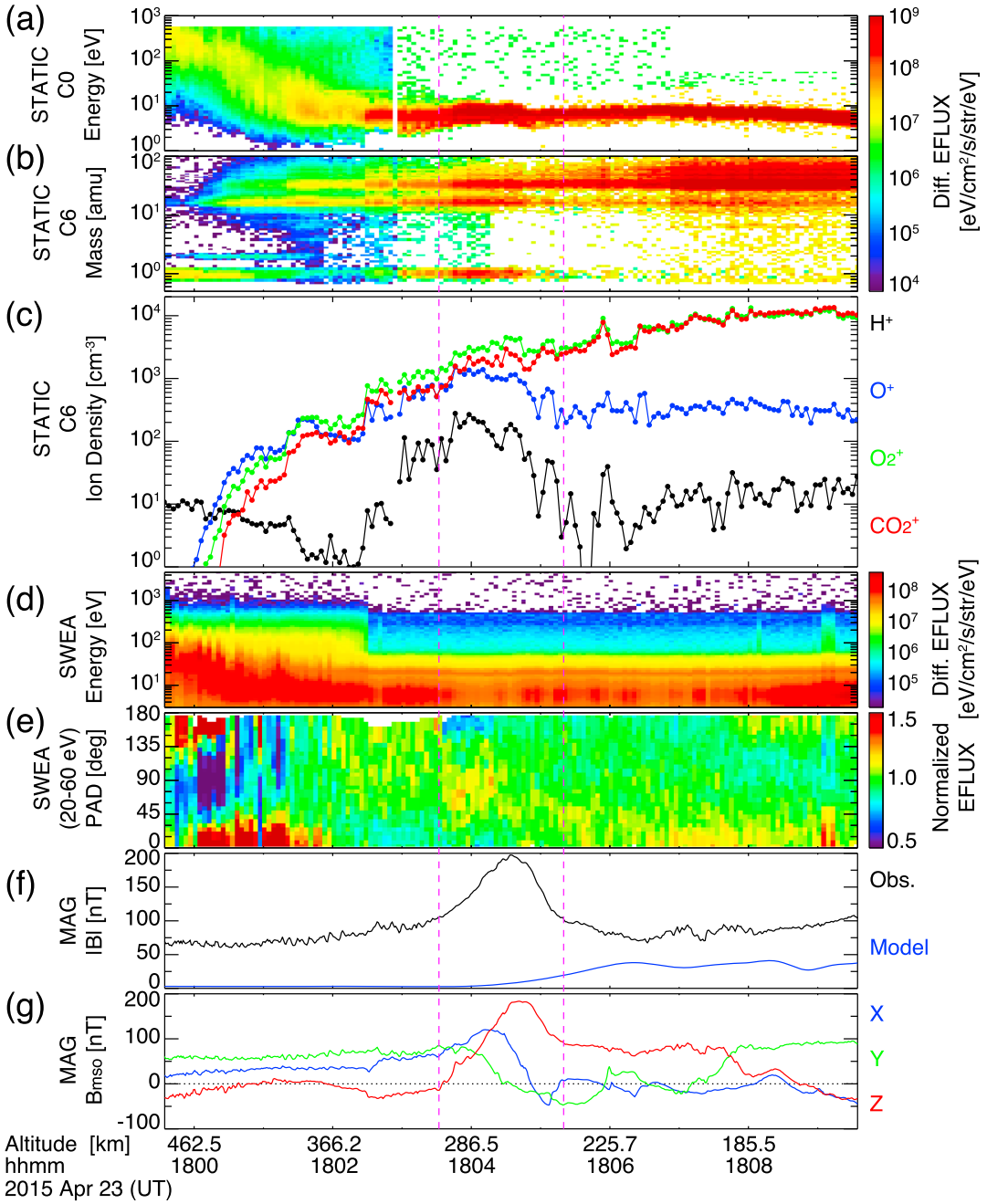

Figure 5. Overview of time series plots of a giant ionospheric flux rope based on the MAVEN observations on 23 April 2015 (Orbit #1094): STATIC ions (a) omnidirectional energy, (b) mass with a unit of differential energy flux, and (c) the estimated ion number densities. SWEA electron measurements of (d) omnidirectional energy spectra and (e) normalized pitch angle distributions (PAD) of ionospheric photoelectrons with energies between 20 and 60 eV. Magnetic field (f) amplitude (black) together with the modeled crustal field (blue) [*Morschhauser et al.*, 2014] and (g) vector components in the MSO coordinates measured by MAG. A giant ionospheric flux rope was observed between two magenta vertical dashed lines.

giant ionospheric flux rope on orbit #1094. During the event, STATIC measured typical ionospheric-origin ion populations with energies around 10 eV in Figure 5a. Since the spacecraft velocity (~4 km/s) around periapsis is typically larger than the local ion thermal velocity and bulk flow velocity, the local ions are highly collimated along the ram direction, resulting in the primary STATIC measurements of low-energy ram ions to be O_2^+ with energies ~2.8 eV without spacecraft charging around the Martian ionosphere

[e.g., *McFadden et al.*, 2015; *Mitchell et al.*, 2016]. Therefore, the spacecraft potentials are about −3 V, inferred from the observed minimum ion energy by STATIC. Figure 5a also indicates that the observed ion energy flux was slightly larger during the event than in the surrounding region. The STATIC ion mass spectra (Figure 5b) apparently shows that multiple planetary ion species including H^+, O^+, O_2^+, and probably CO_2^+ are included inside the flux rope. The plasma β; the ratio of the plasma pressure relative to the magnetic pressure, can be computed to be approximately 0.3 across the structure. This feature is consistent with previous flux rope events detected by MAVEN [*Hara et al.*, 2015, 2016].

Although planetary heavy ions are gradually increasing with decreasing altitude from the Martian-induced magnetosphere to the ionosphere, the H^+ and O^+ densities especially increase inside the flux rope by about an order of magnitude relative to the surrounding region (Figure 5c). Note that the candidate origin of H^+ is both the solar wind and planetary upper atmosphere. However, we confirm that the observed H^+ ions inside the flux rope are of planetary origin, because STATIC measured the H_2^+ ghost peak (not shown) which is a good proxy to judge that the observed protons are of planetary origin [*McFadden et al.*, 2015]. Note also that Figure 5b is displayed after subtracting stragglers from the lowest mass populations, which had the highest contribution to background [*McFadden et al.*, 2015]. Across the flux rope, heavy ions are flowing antisunward with an approximately same bulk flow velocity regardless of species (not shown here). On the other hand, interestingly, protons are flowing slightly different from heavy ions, and sometimes have a sunward bulk flow velocity during the flux rope crossing.

The SWEA electron energy spectra did not show a significant change during the event (Figure 5d). Meanwhile, the electron pitch angle distribution across the structure can provide us with some important clues associated with the local magnetic topologies. Figure 5e displays pitch angle distributions of electrons with energies between 20 and 60 eV, normalized by averaged values for individual SWEA observations. This energy range covers major photoelectron peaks seen in the Martian upper atmosphere around 21–24 eV and 27 eV. The photoelectron pitch angle distributions during the event (Figure 5e) appear weak trapped, i.e., two-sides loss cones, but are not symmetric between parallel and antiparallel to the local magnetic field line. On the other hand, the ionospheric photoelectron peak around 20 eV can be seen in the SWEA electron energy spectra regardless of the pitch angle (not shown here). The loss cones may suggest that the flux rope is linked to the Martian upper atmosphere, so that the photoelectrons can be lost in the loss cones at that time when this event was observed.

4. Spatial Properties of A Giant Ionospheric Flux Rope Reconstructed by the Grad-Shafranov Equation

We applied the Grad-Shafranov reconstruction (GSR) technique to the giant ionospheric flux rope to estimate the axial orientation and two-dimensional spatial structure. The GSR technique assumes that the structure is magnetohydrostatic and time independent [e.g., *Sturrock*, 1994; *Sonnerup and Guo*, 1996]. Previous studies extensively described how to apply the GSR technique to the magnetohydrostatic structures in space [e.g., *Hau and Sonnerup*, 1999; *Hu and Sonnerup*, 2002; *Hasegawa et al.*, 2012]. *Hara et al.* [2015] explained optimal treatments to apply the GSR technique to the Martian flux rope, because MAVEN detected multiple ion species.

Since STATIC operated Conic mode capable of measuring ions with energies between ~0.1 and 500 eV during the flux rope encounter, we used the STATIC "CF" (Conic mode burst) data product at 4 s cadences (see *McFadden et al.* [2015] about the concrete data measurements array), in order to determine the plasma moments including the ion number density, bulk flow velocity, and temperature. As shown in Figure 5a, the observed ion energy across the flux rope is mainly ~10 eV; therefore, we took into account the effect of the spacecraft potential when we computed the ion moments from the STATIC observations. Figure 5a also indicates that the spacecraft velocity is sufficiently faster than the bulk flow velocity of the ambient ionospheric ions. Hence, the spacecraft velocity could be the most dominant component to determine the motion of the observed ionospheric flux rope. Except for the above considerations, we apply the same GSR scheme described in *Hara et al.* [2015] to the observed ionospheric flux rope. It should be mentioned beforehand that these STATIC low-energy ion data calibration has been still ongoing [*McFadden et al.*, 2015]; however, the GSR results (in particular, the flux rope axial orientation and shape) do not significantly change.

Figure 6 summarizes the GSR results for the observed flux rope in the Martian ionosphere. The deHoffmann-Teller (HT) velocity, $\boldsymbol{V}_{HT}$, which is used for the GSR technique to convert the spacecraft time series

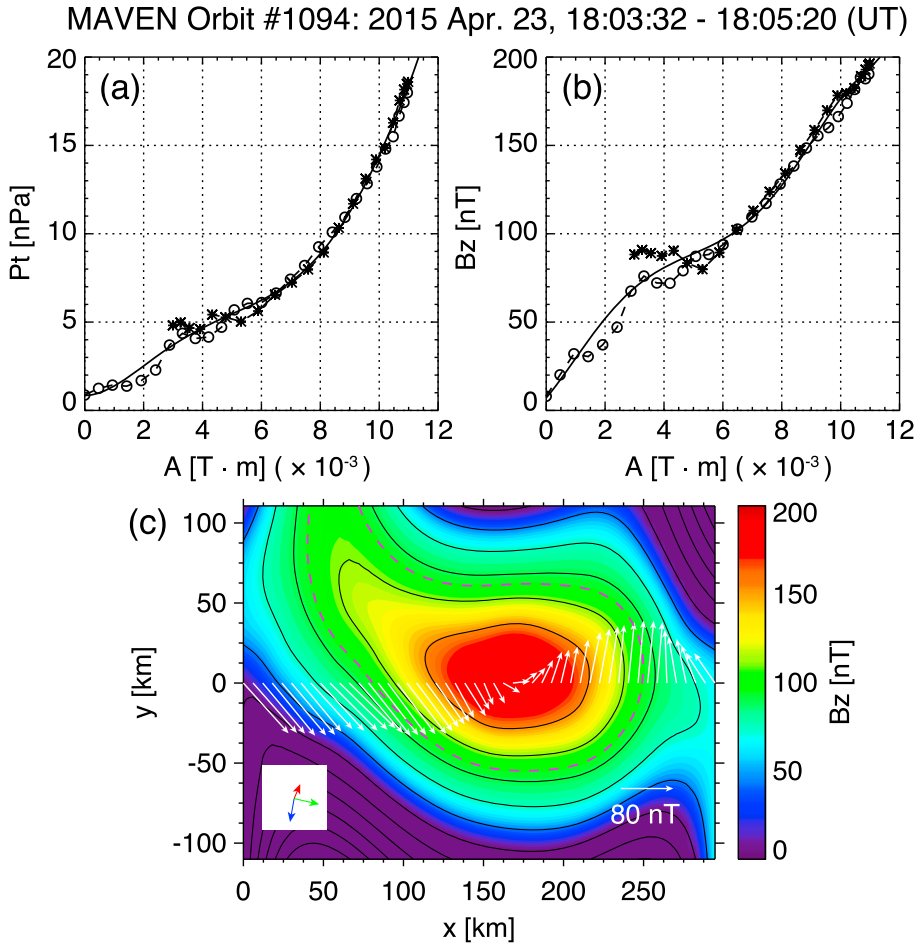

Figure 6. Overview of results from the Grad-Shafranov reconstruction (GSR) technique for a giant ionospheric flux rope on 23 April 2015 (Orbit #1094): (a) Transverse pressure P_t and (b) axial magnetic field B_z profiles as a function of the partial magnetic vector potential A. Open circles are MAVEN observations along the inbound path while asterisks are along the outbound path, and the solid curves denote the fitted polynomials. (c) The recovered two-dimensional axial magnetic field B_z map via the GSR technique based on the MAVEN observations. MAVEN traversed (time progressed) from left to right along $y = 0$. White arrows indicate the transverse magnetic fields measured by MAVEN. The colored arrows shown at the lower left corner on the reconstructed map are the projections of MSO unit vectors: X_{mso} (blue), Y_{mso} (green), and Z_{mso} (red) axes. Overlaid dashed magenta curve is the flux rope boundary. A precise definition is given in text.

data into the spatial information along the spacecraft trajectory moving through the structure, is found to be [−1.15, −2.34, −3.52] km/s in the MSO coordinates. The correlation coefficient for the HT analysis is quite high (cc = 0.996), indicating that we can neglect the effects of motion and temporal evolution of the structure in the HT frame. Furthermore, the Walén slope for the GSR interval is so small (−0.008) that this event turns out to be suitable for applying the GSR technique. As mentioned in section 3, the bulk flow velocity is slightly different between protons and heavy ions during the event; however, a proton density inside the flux rope is so smaller than heavy ions as adequate to apply the GSR technique to the event. Figures 6a and 6b clearly show that the MAVEN data points (open circles/asterisks) can be well fitted by single polynomials (black solid curve), indicating that it is a reasonable assumption that the structure is two dimensional. Figure 6c is a two-dimensional axial field map of the observed ionospheric flux rope recovered by the GSR technique. The invariant (z) axis perpendicular to the reconstructed GSR x-y map in Figure 6c is determined to be [0.458, −0.092, 0.884] in the MSO coordinates; i.e., the flux rope axis is mostly oriented along the $+Z_{mso}$ direction. We found that the angular difference of the estimated flux rope axis between the GSR technique and the MVA turns out to be ~22°, indicating that the flux rope axes inferred from both methods do not have a large difference.

The flux rope boundary overplotted by a dashed magenta curve onto Figure 6c is defined as a surface where the reconstructed axial field strength is 50% relative to the core field value. This definition is the same as *Hara et al.* [2015]. Using the same methodologies as taken by, e.g., *Hara et al.* [2014a, 2014b, 2015], we estimated the spatial scales of the observed ionospheric flux rope. The cross-section area is computed to be $\sim 2.06 \times 10^4$ km^2. Given that the flux rope is strictly a circular shape, a flux rope radius is equivalently ~80.9 km. Assuming that the structure is maintained at least over the period when MAVEN traversed the flux rope, the extent along the flux rope axis is ~203.7 km, which is the MAVEN flight distance in the HT frame. Therefore, the flux rope volume is computed to be at least $\sim 4.19 \times 10^{21}$ cm^3. These results show that the estimated spatial scale is larger than the Martian flux ropes previously recorded by MGS [*Vignes et al.*, 2004; *Briggs et al.*, 2011]; however, it is approximately comparable to a large-scale flux rope event previously observed by MGS downstream from the strong crustal fields [e.g., *Brain et al.*, 2010]. Based on previous studies [e.g., *Qiu et al.*, 2007; *Hu et al.*, 2014], we also compute the toroidal (Φ_t) and poloidal (Φ_p) magnetic flux contained inside the flux rope. Their results turn out to be $\Phi_t \simeq 2.76 \times 10^3$ and $\Phi_p \simeq 9.79 \times 10^2$ Wb, respectively. Note that our defined boundary (a dashed magenta curve in Figure 6c) is not completely closed; therefore, it is partially beyond the reconstructed domain. Hence, the estimated flux rope volume is an underestimate, and the derived spatial properties are lower limits.

5. Possible Formation Process

Figure 7 illustrates a possible formation process of the observed giant ionospheric flux rope based on the axial orientation recovered by the GSR technique. Viewing from Figure 1e on Orbit #1094, local crustal magnetic fields (gray curves in Figure 1e) around the event are typically pointed in the $-Y_{mso}/+Z_{mso}$ directions like black solid arrows in Figure 7a; meanwhile, global-draped magnetic fields, which are inferred from the whiskers directions in Figure 1e far from the event (e.g., either before 18:00 UT or after 18:20 UT), are approximately overlaid in the $+Y_{mso}/-Z_{mso}$ directions like the gray solid arrows in Figure 7b. It indicates that overlaid draped magnetic fields are directed approximately opposite to the local crustal magnetic fields. Therefore, the magnetic configurations favorable for magnetic reconnection are available along the red solid lines in Figure 7c. As shown in Figure 7d, a helical magnetic field structure can be consequently created via multiple *X* line reconnection between the local crustal and overlaid interplanetary magnetic field lines. The resultant flux rope axis (a red arrow in Figure 7d) would be oriented mostly along the $+Z_{mso}$ axis, which is in good agreement with the GSR results. The estimated chirality (handedness) of the flux rope magnetic fields is also consistent with the recovered two-dimensional structure in Figure 6c. Although *Hara et al.* [2014b] also pointed out a possibility of this proposed formation process, our results show stronger evidence for this proposed formation process to operate under the Martian ionosphere.

6. Dependence on Upstream Solar Wind Drivers

As mentioned above, Figure 1e represents that this giant ionospheric flux rope was observed around the subsolar region at a geographic latitude (east longitude) of −29.8°(79.6°). Hence, owing to the orbital configuration, MAVEN was unable to directly measure the upstream solar wind region around this time interval. However, the MAVEN plasma and field observations allow us to roughly deduce the upstream solar wind conditions even though MAVEN did not purely measure the upstream solar wind.

Figure 8 summarizes the estimated solar wind proxies based on the Solar Wind Ion Analyzer (SWIA) [*Halekas et al.*, 2015a], MAG [*Connerney et al.*, 2015], and SWEA [*Mitchell et al.*, 2016] observations, together with the Wang-Sheeley-Arge (WSA)-ENLIL+Cone model [e.g., *Mays et al.*, 2015]. Figures 8a and 8b represent penetrating protons density and velocity recorded by SWIA around every MAVEN closest approaches [*Halekas et al.*, 2015b]. A portion of the solar wind protons charge exchange with the Martian exospheric constituents, resulting in energetic neutral atoms (ENAs) and allowing them to penetrate to low altitudes in the atmosphere, because they do not feel the ambient electromagnetic fields. Some of these ENAs can be converted back to charged particles that can be measured by SWIA around the MAVEN closest approach [*Halekas et al.*, 2015b, 2016]. Since these ENAs can penetrate to low altitudes, maintaining the same velocity as that of solar wind, the penetrating protons velocity (Figure 8b) is the most reliable proxy to determine the upstream solar wind velocity. The penetrating protons density (Figure 8a) is also suitable to infer at least the relative change of the upstream solar wind density. Figure 8c shows the orbital averaged magnetic field amplitude in the magnetosheath, which is also a good proxy to understand the relative change of the IMF strength draped around the

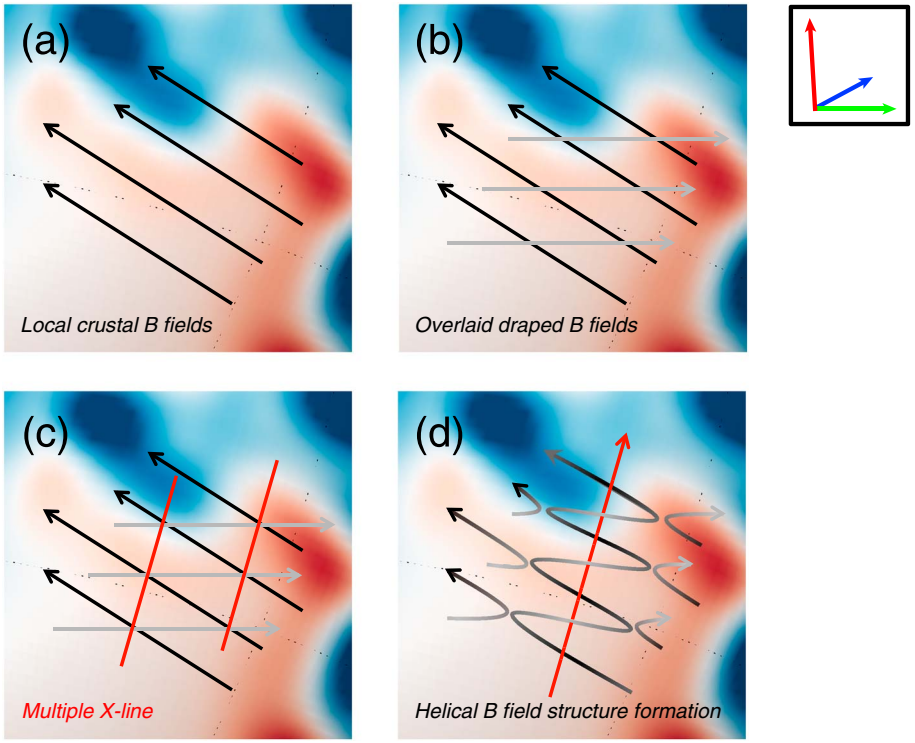

Figure 7. (a–d) Schematic illustrations of a possible formation scenario of the giant ionospheric flux rope observed by MAVEN. Background blue-red contour is the radial component of the modeled crustal magnetic field at 400 km [*Morschhauser et al.*, 2014], projected onto the Martian surface. This crustal field area around the event corresponds around the magenta whiskers of Figure 1e on Orbit #1094. The formation progressed from Figures 7a to 7d. Black solid arrows are local crustal fields. Gray solid arrows are the inferred overlaid IMF draped around the planet. Red solid lines in Figure 7c are the locations where multiple *X* line reconnection is likely driven. A helical flux rope is created in Figure 7d via multiple *X* line reconnection between the local crustal and overlaid interplanetary magnetic field lines. The expected flux rope axis is depicted as a red arrow. The projected MSO orthogonal X_{mso} (blue), Y_{mso} (green), and Z_{mso} (red) axes are shown on the top right corner. The viewing direction is identical to Figure 1e.

planet. On the basis of the automated algorithm well described in *Halekas et al.* [2016], we singled out the time intervals when MAVEN was in the magnetosheath based on the SWIA and MAG measurements. Figure 8d indicates the magnetosheath suprathermal electrons pitch angle distributions averaged over the time intervals for both individual orbital inbound and outbound passes. We automatically chose the intervals whose pitch angle distributions appear to be either field aligned or counterstreaming along the magnetic field line [e.g., *Brain et al.*, 2007], because these suprathermal populations can be presumably due to solar wind "strahl" electrons, which directed outward from the Sun along the interplanetary magnetic field [e.g., *Feldman et al.*, 1975; *Pilipp et al.*, 1987]. Hence, these pitch angle distributions owing to likely solar wind strahl electrons observed in the magnetosheath would be a good tracer to infer the IMF sector polarities; i.e., the IMF draped around the planet has a polarity toward or away from the Sun. Bidirectional streaming suprathermal electrons along the magnetic field line are found around between 23 and 26 April, indicating that they could be traveling in both directions along the ICME closed loop [e.g., *Gosling et al.*, 1987; *Wimmer-Schweingruber et al.*, 2006, and references therein].

At the event (the vertical dashed blue line in Figure 8), an orbital-averaged magnetosheath field strength reached as strong as about 20 nT, which was mostly accompanied with enhancements of the penetrating protons density and velocity. It indicates that the time profile of the estimated upstream solar wind is consistent with that of the typical ICME passage [e.g., *Kataoka and Miyoshi*, 2006]. Recently, comparison studies between the undisturbed solar wind observed by MAVEN and the WSA-ENLIL+Cone model [e.g., *Mays et al.*, 2015] are well performed by *Dewey et al.* [2016]. We thus also compare these solar wind proxies obtained from the MAVEN observations with the WSA-ENLIL+Cone model (overplotted as red curves in Figures 8a–8c). The simulation result also predicted that ICME impacted Mars slightly prior to 23 April 2015 (Figrue 8e). The simulated ICME arrival time was expected to be earlier than the MAVEN observations, because the modeled solar

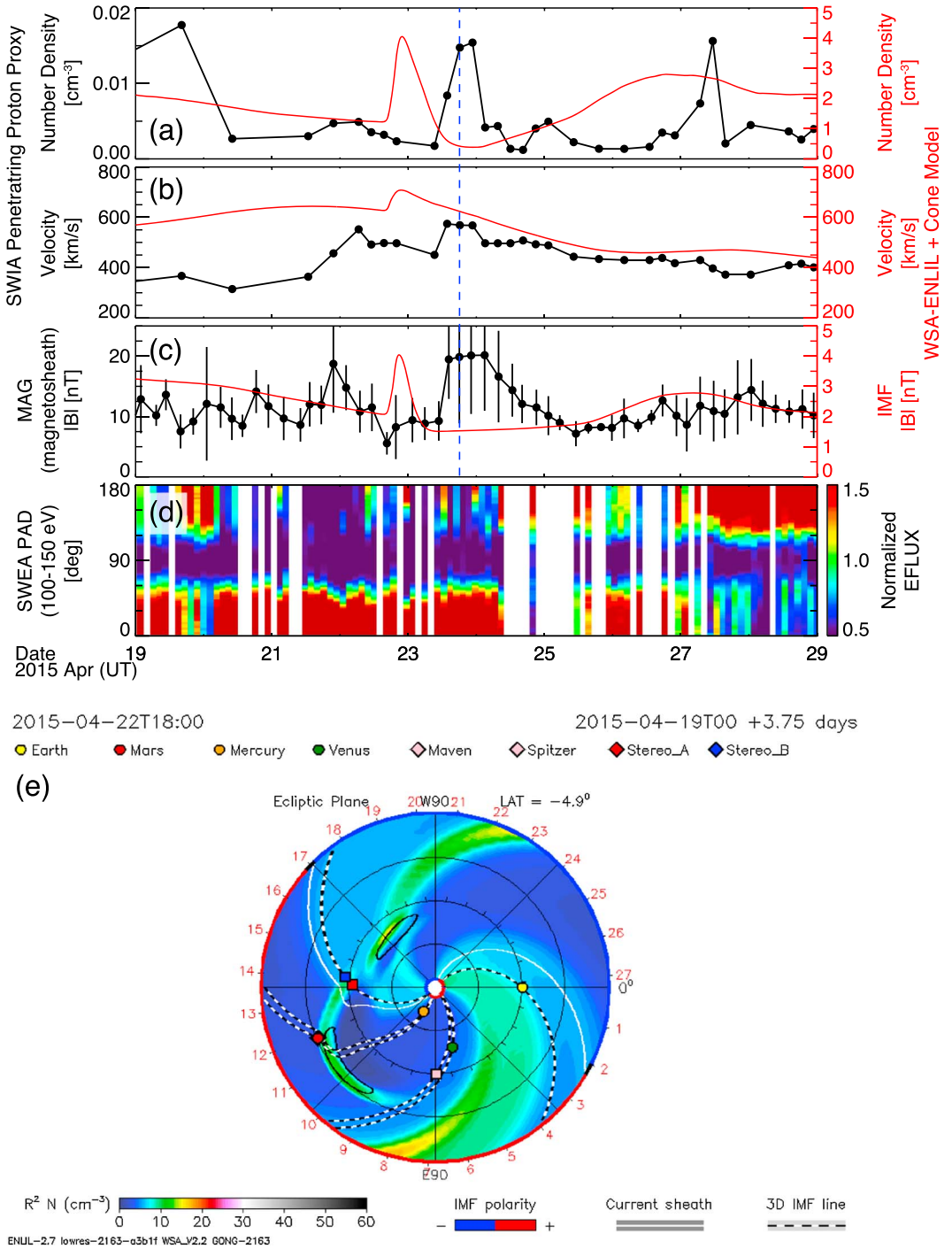

Figure 8. Overviews of the upstream solar wind proxies inferred from the MAVEN observations for 10 days from 19 April 2015. For the left-hand side black axis, the (a) number density and (b) velocity of penetrating protons observed by SWIA around each periapsis, which are good proxies for the upstream solar wind properties [*Halekas et al.*, 2015b], and (c) the orbital averaged magnetic field strength draped around Mars (with standard deviations shown as vertical lines), where MAVEN was in the magnetosheath based on the SWIA and MAG measurements. In addition, the WSA-ENLIL+Cone simulation results at Mars are overplotted as red curves organized in the right-hand side red axis. (d) The normalized pitch angle distributions (PAD) of magnetosheath suprathermal electrons with energies between 100 and 150 eV, averaged for individual orbits of inbound/outbound crossings. A giant ionospheric flux rope was observed at the vertical dashed blue line. (e) WSA-ENLIL+Cone model results for the solar wind density normalized to 1 AU, viewed from the northern ecliptic pole. The location of the spacecraft, planets, and the Sun are depicted by small symbols. Some other heliospheric properties are listed in the bottom legend. ICMEs propagating in the inner heliosphere are outlined as black closed curves.

wind velocity was predicted to be faster than the MAVEN observations during 19–22 April. It suggests that the actual ICME was slower down than the simulation on the way to Mars through the inner heliosphere (see Figure 8b). This result thus indicates that such a disturbed solar wind like the ICME passage can play an important role in creating the observed giant ionospheric flux rope with an axial field of ~200 nT. This is because the IMF draped around the planet could easily penetrate deeper to the low altitude than the usual state, allowing the overlaid IMF to interact with the local crustal magnetic fields. Furthermore, previous studies reported that the magnetic reconnection rates during the ICME passages became high, owing to the low Alfvénic Mach number (or low plasma β) at Earth [e.g., *Farrugia et al.*, 1995; *Phan et al.*, 2013] and Mercury [e.g., *Gershman et al.*, 2013; *Slavin et al.*, 2014]. Therefore, this effect might also contribute in creating the observed giant flux rope around the subsolar region in the Martian ionosphere.

7. Concluding Remarks

In this paper, we obtained the following results based on the MAVEN observations:

1. MAVEN observed a giant ionospheric flux rope with a peak field of ~200 nT around the subsolar region, where the spacecraft was at an altitude of <300 km downstream from the strong crustal fields. The difference between the observed flux rope peak field and modeled crustal field is one of the largest during the MAVEN primary science phase. The event geometrical configuration relative to the neighboring crustal fields is similar to the previous MGS measurements [e.g., *Brain et al.*, 2010; *Hara et al.*, 2014a]. In order to identify that this is really owing to a flux rope, we compared magnetic field measurements among three consecutive 11:2 commensurable orbits (Figures 1–3), that their orbital configurations are similar to the local crustal magnetic field topologies. It is because it takes about two Martian days for MAVEN to orbit Mars 11 times. These comparisons allowed us to ensure that the event shown in this paper is not a stable structure like a crustal magnetic field itself but a transient structure like a flux rope.
2. The flux rope possessed multiple planetary ions including H^+, O^+, O_2^+, and likely CO_2^+, which is consistent with previous MAVEN observations [*Hara et al.*, 2015]. In particular, H^+ and O^+ densities increase inside the flux rope by about an order of magnitude relative to the surrounding region (Figure 5c). Interestingly, ion bulk flow velocities inside the flux rope are slightly different between protons and heavy ions, enabling us to infer a variety of ion sources included inside the flux rope. The photoelectrons pitch angle distribution during the event (Figure 5d) was weakly trapped; however, SWEA measured ionospheric photoelectrons regardless of the pitch angle. The loss cones may suggest that this structure is linked to the Martian upper atmosphere, so that the photoelectrons can be lost in the loss cone at that time when MAVEN observed.
3. We succeeded in uniquely recovering the flux rope spatial properties based on the GSR technique. The spatial scale was estimated to be the order of 100 km, which is comparable to large-scale flux ropes previously observed by MGS downstream from the strong crustal fields [*Brain et al.*, 2010]. The inferred flux rope axis was approximately oriented along the $+Z_{mso}$ direction, indicating that it was created via multiple *X* line reconnection between the local crustal and overlaid interplanetary magnetic fields draped around Mars (Figure 7). This formation process was previously proposed by *Hara et al.* [2014b]. Hence, these MAVEN observations can convincingly show that this formation process surely operated under the Martian plasma environment.
4. Figure 8 suggested that the giant ionospheric flux rope was detected when an ICME impacted Mars. Hence, ICME can play an important role in creating the observed giant ionospheric flux rope with an axial field of ~200 nT in the Martian ionosphere, because the IMF draped around the planet was allowed to penetrate deeper than the usual state, resulting in the strong interaction between the local crustal and overlaid interplanetary magnetic fields. This result clearly suggests that the variable upstream solar wind properties are an important factor to create magnetic flux ropes in the Martian plasma environment.

This observed ionospheric flux rope was observed around the subsolar point during the ICME passage; therefore, the plasma pressure in the Martian dayside-induced magnetosphere, located on the upper side of the observed ionospheric flux rope, was expected to be enhanced than that under the usual state. It indicates that the pressure gradients across the boundaries of the flux rope were also enhanced. This factor likely allows the observed ionospheric flux rope to be "giant" with a peak field of ~200 nT.

The behaviors of the modeled crustal field among the commensurable orbits (blue lines in Figures 1b, 2b, and 3b) appear different even though the orbital geographic configurations are so close (see Figures 1a, 2a, and 3a or Figures 1e, 2e, and 3e). On the one hand, the GSR results shown in section 4 suggest that the typical

spatial scale of the observed giant ionospheric flux rope is about a few hundred kilometers, which can sufficiently cover the area where MAVEN traversed during these commensurable orbits. Given that this magnetic field enhancement during the Orbit #1094 (Figure 1b) was a locally stationary structure like a crustal field itself, MAVEN should also detect a portion of such a magnetic field enhancement at least in adjacent commensurable orbits (Figures 2 and 3), but MAVEN could not at all. Hence, it is natural to conclude that the observed magnetic field enhancement is not owing to a stable structure but a transient structure like a flux rope.

We could not measure any flux rope signatures on Orbit #1105 which was the next "commensurable" orbit (see Figure 3b), indicating that this structure had to disappear within two Martian days at least. Without physical mechanisms to maintain the structure, one possible interpretation is that the fate of the observed giant flux rope should be detached from the planet resulting in a presumable escape into interplanetary space. Therefore, the structure can be one of the ion bulk removal processes from Mars. Based on the STATIC ion measurements together with the GSR results, the observed giant flux rope was filled with planetary ions of $\sim 2.41 \times 10^{25}$ ions including H^+, O^+, O_2^+, and CO_2^+. Assuming that all ions were completely removed within the duration (~59.5 s) when MAVEN crossed the structure, the potential ion escape rate owing to a single ionospheric flux rope is estimated to be $\sim 4.04 \times 10^{23}$ ions/s, which can instantaneously contribute approximately 10% of the global present ion escape rate from Mars during the solar minimum [e.g., *Lundin et al.*, 2008; *Nilsson et al.*, 2011; *Brain et al.*, 2015]. This potential ion escape rates due to the ionospheric flux ropes are thus consistent with the previous MGS estimations [e.g., *Hara et al.*, 2014a, 2014b]. However, future investigations on how often these ionospheric flux ropes are created and detached are needed to quantitatively understand how much ionospheric flux ropes can contribute to the ion escape rates from Mars.

An alternative interpretation is that the flux rope can unwind and diffuse into the ionosphere below the spacecraft. *Luhmann et al.* [1984] estimated that a large-scale field in the Venus ionosphere disappears with a time scale of the order of minutes to hours, depending on the vertical convection velocity of the ionospheric plasma. This decay time is sufficiently shorter than two Martian days. An upcoming global numerical simulation with high spatiotemporal resolution, such as a time-dependent MHD model around Mars [e.g., *Fang et al.*, 2015], might provide us with some implications to understand how the observed ionospheric flux rope evolves (or collapses) in the Martian plasma environment.

Acknowledgments
The MAVEN data used in this paper are publicly available in NASA's Planetary Data System (http://ppi.pds.nasa.gov/mission/MAVEN). Analysis of SWEA data was partially supported by CNES. T. Hara thanks C.O. Lee for helpful discussions with respect to the space weather events observed by MAVEN. G.A. DiBraccio was supported by a NASA Postdoctoral Program appointment at the NASA Goddard Space Flight Center, administered by Universities Space Research Association through a contract with NASA. Simulation results have been provided by the Community Coordinated Modeling Center at Goddard Space Flight Center through their real-time runs system (http://ccmc.gsfc.nasa.gov). The WSA model was developed by N. Arge at AFRL, and the ENLIL Model was developed by D. Odstrcil at GMU.

References

Acuña, M. H., et al. (1998), Magnetic field and plasma observations at Mars: Initial results of the Mars Global Surveyor mission, *Science*, *279*, 1676–1680, doi:10.1126/science.279.5357.1676.

Acuña, M. H., et al. (1999), Global distribution of crustal magnetization discovered by the Mars Global Surveyor MAG/ER experiment, *Science*, *284*, 790–793, doi:10.1126/science.284.5415.790.

Albee, A. L., R. E. Arvidson, F. Palluconi, and T. Thorpe (2001), Overview of the Mars Global Surveyor mission, *J. Geophys. Res.*, *106*(E12), 23,291–23,316, doi:10.1029/2000JE001306.

Beharrell, M. J., and J. A. Wild (2012), Stationary flux ropes at the southern terminator of Mars, *J. Geophys. Res.*, *117*, A12212, doi:10.1029/2012JA017738.

Brain, D. A., D. L. Mitchell, and J. S. Halekas (2006), The magnetic field draping direction at Mars from April 1999 through August 2004, *Icarus*, *182*, 464–473, doi:10.1016/j.icarus.2005.09.023.

Brain, D. A., R. J. Lillis, D. L. Mitchell, J. S. Halekas, and R. P. Lin (2007), Electron pitch angle distributions as indicators of magnetic field topology near Mars, *J. Geophys. Res.*, *112*, A09201, doi:10.1029/2007JA012435.

Brain, D. A., A. H. Baker, J. Briggs, J. P. Eastwood, J. S. Halekas, and T.-D. Phan (2010), Episodic detachment of Martian crustal magnetic fields leading to bulk atmospheric plasma escape, *Geophys. Res. Lett.*, *37*, L14108, doi:10.1029/2010GL043916.

Brain, D. A., et al. (2015), The spatial distribution of planetary ion fluxes near Mars observed by MAVEN, *Geophys. Res. Lett.*, *42*, 9142–9148, doi:10.1002/2015GL065293.

Briggs, J. A., D. A. Brain, M. L. Cartwright, J. P. Eastwood, and J. S. Halekas (2011), A statistical study of flux ropes in the Martian magnetosphere, *Planet. Space Sci.*, *59*, 1498–1505, doi:10.1016/j.pss.2011.06.010.

Cain, J. C., B. B. Ferguson, and D. Mozzoni (2003), An $n = 90$ internal potential function of the Martian crustal magnetic field, *J. Geophys. Res.*, *108*, 5008, doi:10.1029/2000JE001487.

Cloutier, P. A., et al. (1999), Venus-like interaction of the solar wind with Mars, *Geophys. Res. Lett.*, *26*(17), 2685–2688, doi:10.1029/1999GL900591.

Connerney, J. E. P., J. Espley, P. Lawton, S. Murphy, J. Odom, R. Oliversen, and D. Sheppard (2015), The MAVEN magnetic field investigation, *Space Sci. Rev.*, *195*, 257–291, doi:10.1007/s11214-015-0169-4.

Dewey, R. M., D. N. Baker, M. L. Mays, D. A. Brain, B. M. Jakosky, J. S. Halekas, J. E. P. Connerney, D. Odstrcil, J. G. Luhmann, and C. O. Lee (2016), Continuous solar wind forcing knowledge: Providing continuous conditions at Mars with the WSA-ENLIL + Cone model, *J. Geophys. Res. Space Physics*, *121*, 6207–6222, doi:10.1002/2015JA021941.

DiBraccio, G. A., et al. (2015), Magnetotail dynamics at Mars: Initial MAVEN observations, *Geophys. Res. Lett.*, *42*, 8828–8837, doi:10.1002/2015GL065248.

Fang, X., Y. Ma, D. Brain, Y. Dong, and R. Lillis (2015), Control of Mars global atmospheric loss by the continuous rotation of the crustal magnetic field: A time-dependent MHD study, *J. Geophys. Res. Space Physics*, *120*, 10,926–10,944, doi:10.1002/2015JA021605.

Farrugia, C. J., N. V. Erkaev, H. K. Biernat, and L. F. Burlaga (1995), Anomalous magnetosheath properties during Earth passage of an interplanetary magnetic cloud, *J. Geophys. Res.*, *100*, 19,245–19,258, doi:10.1029/95JA01080.

Feldman, W. C., J. R. Asbridge, S. J. Bame, M. D. Montgomery, and S. P. Gary (1975), Solar wind electrons, *J. Geophys. Res.*, *80*, 4181–4196, doi:10.1029/JA080i031p04181.

Gershman, D. J., J. A. Slavin, J. M. Raines, T. H. Zurbuchen, B. J. Anderson, H. Korth, D. N. Baker, and S. C. Solomon (2013), Magnetic flux pileup and plasma depletion in Mercury's subsolar magnetosheath, *J. Geophys. Res. Space Physics*, *118*, 7181–7199, doi:10.1002/2013JA019244.

Gosling, J. T., D. N. Baker, S. J. Bame, W. C. Feldman, R. D. Zwickl, and E. J. Smith (1987), Bidirectional solar wind electron heat flux events, *J. Geophys. Res.*, *92*, 8519–8535, doi:10.1029/JA092iA08p08519.

Halekas, J. S., E. R. Taylor, G. Dalton, G. Johnson, D. W. Curtis, J. P. McFadden, D. L. Mitchell, R. P. Lin, and B. M. Jakosky (2015a), The solar wind ion analyzer for MAVEN, *Space Sci. Rev.*, *195*, 125–151, doi:10.1007/s11214-013-0029-z.

Halekas, J. S., et al. (2015b), MAVEN observations of solar wind hydrogen deposition in the atmosphere of Mars, *Geophys. Res. Lett.*, *42*, 8901–8909, doi:10.1002/2015GL064693.

Halekas, J. S., et al. (2016), Structure, dynamics, and seasonal variability of the Mars-solar wind interaction: MAVEN solar wind ion analyzer inflight performance and science results, *J. Geophys. Res. Space Physics*, *121*, doi:10.1002/2016JA023167, in press.

Hara, T., K. Seki, H. Hasegawa, D. A. Brain, K. Matsunaga, and M. H. Saito (2014a), The spatial structure of Martian magnetic flux ropes recovered by the Grad-Shafranov reconstruction technique, *J. Geophys. Res. Space Physics*, *119*, 1262–1271, doi:10.1002/2013JA019414.

Hara, T., K. Seki, H. Hasegawa, D. A. Brain, K. Matsunaga, M. H. Saito, and D. Shiota (2014b), Formation processes of flux ropes downstream from Martian crustal magnetic fields inferred from Grad-Shafranov reconstruction, *J. Geophys. Res. Space Physics*, *119*, 7947–7962, doi:10.1002/2014JA019943.

Hara, T., et al. (2015), Estimation of the spatial structure of a detached magnetic flux rope at Mars based on simultaneous MAVEN plasma and magnetic field observations, *Geophys. Res. Lett.*, *42*, 8933–8941, doi:10.1002/2015GL065720.

Hara, T., et al. (2016), MAVEN observations of magnetic flux ropes with a strong field amplitude in the Martian magnetosheath during the ICME passage on 8 March 2015, *Geophys. Res. Lett.*, *43*(10), 4816–4824, doi:10.1002/2016GL068960.

Hasegawa, H., et al. (2010), Evidence for a flux transfer event generated by multiple X-line reconnection at the magnetopause, *Geophys. Res. Lett.*, *37*, L16101, doi:10.1029/2010GL044219.

Hasegawa, H., H. Zhang, Y. Lin, B. U. Ö. Sonnerup, S. J. Schwartz, B. Lavraud, and Q.-G. Zong (2012), Magnetic flux rope formation within a magnetosheath hot flow anomaly, *J. Geophys. Res.*, *117*, A09214, doi:10.1029/2012JA017920.

Hau, L.-N., and B. U. Ö. Sonnerup (1999), Two-dimensional coherent structures in the magnetopause: Recovery of static equilibria from single-spacecraft data, *J. Geophys. Res.*, *104*, 6899–6918, doi:10.1029/1999JA900002.

Hu, Q., and B. U. Ö. Sonnerup (2002), Reconstruction of magnetic clouds in the solar wind: Orientations and configurations, *J. Geophys. Res.*, *107*(A7), 1142, doi:10.1029/2001JA000293.

Hu, Q., J. Qiu, B. Dasgupta, A. Khare, and G. M. Webb (2014), Structures of interplanetary magnetic flux ropes and comparison with their solar sources, *Astrophys. J.*, *793*(53), doi:10.1088/0004-637X/793/1/53.

Imber, S. M., J. A. Slavin, S. A. Boardsen, B. J. Anderson, H. Korth, R. L. McNutt, and S. C. Solomon (2014), MESSENGER observations of large dayside flux transfer events: Do they drive Mercury's substorm cycle?, *J. Geophys. Res. Space Physics*, *119*, 5613–5623, doi:10.1002/2014JA019884.

Jakosky, B. M., et al. (2015), The Mars atmosphere and volatile evolution (MAVEN) mission, *Space Sci. Rev.*, *195*, 3–48, doi:10.1007/s11214-015-0139-x.

Jasinski, J. M., J. A. Slavin, C. S. Arridge, G. Poh, X. Jia, N. Sergis, A. J. Coates, G. H. Jones, and J. H. Waite (2016), Flux transfer event observation at Saturn's dayside magnetopause by the Cassini spacecraft, *Geophys. Res. Lett.*, *43*, 6713–6723, doi:10.1002/2016GL069260.

Kataoka, R., and Y. Miyoshi (2006), Flux enhancement of radiation belt electrons during geomagnetic storms driven by coronal mass ejections and corotating interaction regions, *Space Weather*, *4*, S09004, doi:10.1029/2005SW000211.

Luhmann, J. G., C. T. Russell, and R. C. Elphic (1984), Time scales for the decay of induced large-scale magnetic fields in the Venus ionosphere, *J. Geophys. Res.*, *89*, 362–368, doi:10.1029/JA089iA01p00362.

Lundin, R., S. Barabash, M. Holmström, H. Nilsson, M. Yamauchi, M. Fränz, and E. M. Dubinin (2008), A comet-like escape of ionospheric plasma from Mars, *Geophys. Res. Lett.*, *35*, L18203, doi:10.1029/2008GL034811.

Mays, M. L., et al. (2015), Ensemble modeling of CMEs using the WSA-ENLIL+Cone model, *Sol. Phys.*, *290*, 1775–1814, doi:10.1007/s11207-015-0692-1.

McFadden, J. P., et al. (2015), MAVEN suprathermal and thermal ion compostion (STATIC) instrument, *Space Sci. Rev.*, *195*, 199–256, doi:10.1007/s11214-015-0175-6.

Mitchell, D. L., et al. (2016), The MAVEN solar wind electron analyzer, *Space Sci. Rev.*, *200*, 495–528, doi:10.1007/s11214-015-0232-1.

Morgan, D. D., D. A. Gurnett, F. Akalin, D. A. Brain, J. S. Leisner, F. Duru, R. A. Frahm, and J. D. Winningham (2011), Dual-spacecraft observation of large-scale magnetic flux ropes in the Martian ionosphere, *J. Geophys. Res.*, *116*, A02319, doi:10.1029/2010JA016134.

Morschhauser, A., V. Lesur, and M. Grott (2014), A spherical harmonic model of the lithospheric magnetic field of Mars, *J. Geophys. Res. Planets*, *119*, 1162–1188, doi:10.1002/2013JE004555.

Nilsson, H., N. J. T. Edberg, G. Stenberg, S. Barabash, M. Holmström, Y. Futaana, R. Lundin, and A. Fedorov (2011), Heavy ion escape from Mars, influence from solar wind conditions and crustal magnetic fields, *Icarus*, *215*, 475–484, doi:10.1016/j.icarus.2011.08.003.

Phan, T. D., G. Paschmann, J. T. Gosling, M. Oieroset, M. Fujimoto, J. F. Drake, and V. Angelopoulos (2013), The dependence of magnetic reconnection on plasma β and magnetic shear: Evidence from magnetopause observations, *Geophys. Res. Lett.*, *40*, 11–16, doi:10.1029/2012GL054528.

Pilipp, W. G., K.-H. Muehlhaeuser, H. Miggenrieder, M. D. Montgomery, and H. Rosenbauer (1987), Characteristics of electron velocity distribution functions in the solar wind derived from the HELIOS plasma experiment, *J. Geophys. Res.*, *92*, 1075–1092, doi:10.1029/JA092iA02p01075.

Qiu, J., Q. Hu, T. A. Howard, and V. B. Yurchyshyn (2007), On the magnetic flux budget in low-corona magnetic reconnection and interplanetary coronal mass ejections, *Astrophys. J.*, *659*, 758–772, doi:10.1086/512060.

Rong, Z. J., W. X. Wan, C. Shen, T. L. Zhang, A. T. Y. Lui, Y. Wang, M. W. Dunlop, Y. C. Zhang, and Q.-G. Zong (2013), Method for inferring the axis orientation of cylindrical magnetic flux rope based on single-point measurement, *J. Geophys. Res. Space Physics*, *118*, 271–283, doi:10.1029/2012JA018079.

Russell, C. T., and R. C. Elphic (1979a), Observation of magnetic flux ropes in the Venus ionosphere, *Nature*, *279*, 616–618, doi:10.1038/279616a0.

Russell, C. T., and R. C. Elphic (1979b), ISEE observations of flux transfer events at the dayside magnetopause, *Geophys. Res. Lett.*, *6*, 33–36, doi:10.1029/GL006i001p00033.

Slavin, J. A., et al. (2009), MESSENGER observations of magnetic reconnection in Mercury's magnetosphere, *Science*, *324*(5927), 606–610, doi:10.1126/science.1172011.

Slavin, J. A., et al. (2014), MESSENGER observations of Mercury's dayside magnetosphere under extreme solar wind conditions, *J. Geophys. Res. Space Physics*, *119*, 8087–8116, doi:10.1002/2014JA020319.
Sonnerup, B. U. Ö., and M. Guo (1996), Magnetopause transects, *Geophys. Res. Lett.*, *23*, 3679–3682, doi:10.1029/96GL03573.
Sonnerup, B. U. Ö., and M. Scheible (1998), Minimum and maximum variance analysis, *ISSI Sci. Rep. Ser.*, *1*, 185–220.
Soobiah, Y. I. J., J. A. Wild, M. J. Beharrell, S. Barabash, R. J. Lillis, D. L. Mitchell, A. J. Coates, J. D. Winningham, and R. A. Frahm (2014), Properties of a large-scale flux rope and current sheet region on the dayside of Mars: MGS MAG/ER and MEX ASPERA-3 ELS observations, *Icarus*, *242*, 297–315, doi:10.1016/j.icarus.2014.08.019.
Sturrock, P. A. (1994), *Plasma Physics: An Introduction to the Theory of Astrophysical, Geophysical and Laboratory Plasmas*, Stanford-Cambridge program, Cambridge Univ. Press, Cambridge.
Vignes, D., M. H. Acuña, J. E. P. Connerney, D. H. Crider, H. Rème, and C. Mazelle (2004), Magnetic flux ropes in the Martian atmosphere: Global characteristics, *Space Sci. Rev.*, *111*, 223–231, doi:10.1023/B:SPAC.0000032716.21619.f2.
Walker, R. J., and C. T. Russell (1985), Flux transfer events at the Jovian magnetopause, *J. Geophys. Res.*, *90*, 7397–7404, doi:10.1029/JA090iA08p07397.
Wimmer-Schweingruber, R. F., et al. (2006), Understanding interplanetary coronal mass ejection signatures, *Space Sci. Rev.*, *123*, 177–216, doi:10.1007/s11214-006-9017-x.
Xiao, C. J., Z. Y. Pu, Z. W. Ma, S. Y. Fu, Z. Y. Huang, and Q. G. Zong (2004), Inferring of flux rope orientation with the minimum variance analysis technique, *J. Geophys. Res.*, *109*, A11218, doi:10.1029/2004JA010594.